Anal. Chem. **2000,** *72,* 323−332

On-Column Visualization of Sample Migration in Liquid Chromatography

R. Andrew Shalliker,† B. Scott Broyles, and Georges Guiochon*

Department of Chemistry, The University of Tennessee, Knoxville, Tennessee 37996-1600, and Chemical and Analytical Sciences Division, Oak Ridge National Laboratory, Oak Ridge, Tennessee 37831-6120

A quantitative on-column visualization technique for evaluating solute migration in liquid chromatography columns was described. This technique employed a matched refraction index phase system in high-pressure glass columns. In this case, the mobile phase was carbon tetrachloride and the stationary phase was a C18 silica. Because the refractive indexes of the two phases were the same, the column bed, otherwise opaque, was transparent to the eye. Zones of colored solutes could be injected (iodine for instance) and their migration studied along the column. Photographing the sample band during its migration allowed chromatographic information to be extracted using digital technology. As an example of applications for this technique, we show the sample entry through various inlet fittings. The results demonstrate that chromatographers should pay more attention to the selection of inlet frits. Importantly, the frit porosity should be matched to the particle size of the packing.

Chromatographers have long wished to see inside a chromatography column, hoping to find there ready explanations for poor or unusual zone behavior. Numerous attempts were made in the past to develop a useful visualization method. Several authors introduced dye samples in the columns, interrupted the mobile-phase flow rate before elution of the bands to extrude the bed from the column, cut it, and examined the sections.[1−4] This method reveals problems related to injection and/or packing method, but it gives no information regarding the dynamics of the band elution and broadening processes and is not compatible with accurate measurements, the bed being deformed during its extraction from the column.

Today's chromatographers have at their disposal two techniques that allow visualization of the chromatographic process as it takes place inside the chromatography column. Indirectly, various methods of NMR imaging allow the computer calculation of images of sample bands[5,6] or the tracking of mobile-phase components[7] within the column. Information on the bed structure,[7] band-broadening contributions by peripheral fittings,[5,6] or studies of processes such as viscous fingering[8−11] was reported. However, NMR, while allowing the acquisition of useful information, suffers in some respects with regard to cost and spatial resolution. To obtain three-dimensional images, complex computer manipulation of the raw NMR data is required and the sample collection times can be quite long. These factors limit the everyday use of NMR for chromatographers not equipped with a large budget.

An optical method of on-column visualization was recently developed as a quantitative tool. It uses a phase system of matched refractive indexes.[12] In this method, columns are prepared in glass containers designed for use under high pressures. A mobile phase with the same refractive index as that of the stationary phase is employed. The bed becomes transparent to the eye, and visualization of colored sample bands can be obtained. The technique was used to study, among other things, viscous fingering[12,13] and the infinite-diameter column.[12,14] This process of band visualization is cost-effective, requiring little in the way of instrumentation other than conventional chromatographic systems, a modern PC, good camera equipment, and suitable image analysis software.[12] The technique offers good spatial resolution and allows for the observation of band migration in three dimensions.[12] The method was first used in the 1970s by Kirkland,[15] but it could not have been developed then into a useful method of on-column analysis because limitations in taking and handling photographs and in computing useful parameters did not allow for chromatographic data to be easily extracted from a photographic image. As a result, this visualization process was largely forgotten. However, in today's age of powerful PCs and digital technology, useful information can readily be obtained from optical or digital photographs.

In this work, we discuss the quantitation of the process of on-column visualization using the matched refractive index technique.

† Present address: Faculty of Science and Technology, CBBR, University of Western Sydney, Hawkesbury, Richmond, NSW, 2753, Australia.

(1) Klawiter, J.; Kamiński, M.; Kowalczyk, J. S. *J. Chromatogr.* **1982**, *243*, 207.
(2) Kamiński, M.; Klawiter, J.; Kowalczyk, J. S. *J. Chromatogr.* **1982**, *243*, 225.
(3) Colin, H. In *Preparative and Production Scale Chromatography*; Ganetsos, G., Barker, P. E., Eds., M. Dekker: New York, 1993.
(4) Yun, T.; Guiochon, G. *J. Chromatogr., A* **1997**, *760*, 17.
(5) Bayer, E.; Müller, W.; Ilg, M.; Albert, K. *Angew. Chem., Int. Ed. Engl.* **1989**, *28*, 1029.
(6) Bayer, E.; Baumeister, E.; Tallarek, U.; Albert, K.; Guiochon, G. *J. Chromatogr., A* **1995**, *704*, 37.
(7) Tallarek, U.; Albert, K.; Bayer, E.; Guiochon, G. *AIChE J.* **1996**, *42*, 3041.
(8) Plante, L.; Romano, P.; Fernandez, E. *Chem. Eng. Sci.* **1994**, *49*, 2229.
(9) Dickson, M.; Norton, T.; Fernandez, E. *AIChE J.* **1997**, *43*, 409.
(10) Fernandez, E.; Norton, T.; Jung, W.; Tsavalas, J. *Biotechnol. Prog.* **1996**, *12*, 480.
(11) Fernandez, E.; Grotegut, C.; Braun, G. *Phys. Fluids* **1995**, *7*, 468.
(12) Shalliker, R. A.; Broyles, B. S.; Guiochon, G. *J. Chromatogr., A* **1998**, 826, 1.
(13) Broyles, B. S.; Shalliker, R. A.; Cherrak, D. E.; Guiochon, G. *J. Chromatogr., A* **1998**, 822, 173.
(14) Shalliker, R. A.; Broyles, B. S.; Guiochon, G. *J. Chromatogr., A* **1999**, *855*, 367.
(15) Kirkland, J. J. In *Proceedings of the First Philip Morris Scientific Symposium*; Fina, N. J., Ed.; Philip Morris: New York, 1973.

10.1021/ac990370+ CCC: $19.00
Published on Web 12/16/1999

We show how a simple calibration process allows the derivation of axial and radial concentration profiles from the photographic intensity. Following, we illustrate the use of the technique by observing sample distribution as a function of the characteristics of the inlet frit.

EXPERIMENTAL SECTION

Chemicals. All solvents were used as supplied from the manufacturers. Reagent grade carbon tetrachloride was purchased from The Sigma Chemical Co. (St. Louis, MO). HPLC grade dichloromethane and HPLC grade methanol were obtained from Fisher Scientific (Fairlay, NJ). Iodine (99.9%) was obtained from General Chemical Division (New York, NY). The chromatographic stationary phase used was YMC 15−30 μm C18 chemically bonded silica (YMC, Wilmington, NC). Attentive care must be exercised when handling carbon tetrachloride due to its toxic and carcinogenic effects. All work was performed in a well-ventilated hood and protective precautions taken as prescribed by the Material Safety Data Sheet (MSDS).

Columns. All chromatographic experiments were performed on a 100 × 17 mm (i.d.) borosilicate (Pyrex) glass column supplied by Omni (Cambridge, U.K.). The column end fittings were prepared by the University of Tennessee workshop and machined from Delrin plastic. These fittings included a fixed-length outlet fitting and an adjustable inlet fitting that allowed axial compression of the column. Stainless steel frits having a diameter of 15.9 mm and a thickness of 1.57 mm were obtained from Bodman (Aston, PA). High molecular weight polyethylene frits having a diameter of 4.6 mm and a thickness of 1.57 mm were obtained from Upchurch Scientific (Oak Harbor, WA).

The stationary phase used was YMC C18 silica (Kyoto-Fu 613, Japan). This material is spherical with a particle size distribution given as 15−30 μm and an average particle size of 21 μm. The column was slurry packed in a downward configuration using conditions previously described.[12−14,16] To improve visualization and minimize the cylindrical lens effect, the entire column assembly was placed into an in-house prepared, rectangular, box-shaped, viewing cell filled with what was initially intended to be carbon tetrachloride (n = 1.460). For occupational safety reasons, and because the optical distortion due to the cylindrical lens effect is a function of the difference of the indexes of the solvent in the column and the solvent in the viewing box (see later), much less toxic dichloromethane (n = 1.424) was used instead. The cell assembly was described previously.[12]

Sample Injection. Unless otherwise specified, iodine dissolved in carbon tetrachloride (12 g/L) was used as the probe solute. At this concentration, the solute zone is sufficiently colored and allows the detailed observation of the zones obtained upon the injection of the small volumes, i.e., 20 μL, used in this work, during their entire elution. Sample injection was achieved using a Rheodyne 7010 injection valve with a 20 μL loop. Iodine is not retained on C18 silica with CCl_4 as the eluent.

Equipment. The chromatographic system consisted of two high-performance liquid chromatographic (HPLC) pumps (model 510, Waters Associates, Milford, MA) controlled by a Waters automated gradient controller. The mobile phase was 100% carbon tetrachloride, and the flow rate 1.5 mL/min throughout. Sample injection was achieved through a Rheodyne injection valve (model 7010, Rheodyne, Cotati, CA). Sample visualization of the band profiles was achieved using two Pentax ZX-M SLR 35 mm cameras fitted, one with a Promaster 100 mm macrolens, the other with a Makinon 80−200 mm macrozoom lens. Kodak Ektachrome 200 ASA Professional slide film was used throughout. The photographic images were digitized using a Nikon CoolScan II (Nikon Inc. Melville, New York, NY) film scanner. All images were acquired at the maximum resolution of the scanner (2700 dots/in.). Adobe Photoshop 5.0 (Adobe Systems Inc., San Jose, CA) was used to perform image manipulation. Further analysis was done using SigmaScan Pro 4.01 (Jandel Scientific, San Rafael, CA) image analysis software.

DATA ANALYSIS

To derive true chromatographic data, that is, the concentration distribution of the sample across the column, from the migration zone of a sample that is visible to the naked eye, six successive steps need to be followed.

1. Photographing the Sample Zone. Two cameras mounted at right angles allow collection of data that represent the three-dimensional sample migration. Each camera requires macro-capabilities. Shutter speeds faster than 1/60th of a second eliminate any effects due to sample movement at flow rates possible in the glass column. Apertures should be set near the optimum for the type of film and lens combination, in this case f/11 to f/16. Professional color slide film (ASA 200) is manufactured and maintained in a controlled environment, yielding a product with a guaranteed performance outcome. In systematic studies similar to the one reported here, but carried out with different films and filters, it was found that the combination of a color slide film and an FL-D lens filter utilized in this study gave the best compromise for the photographic requirements. Further details can be found in a previous publication.[12]

2. Converting the Photographic Image of the Zone into a Digital Image. Digital images can be obtained either by using a digital camera or by scanning a photographic image with a digital scanner. In our laboratory, we use the latter process. Slide film can be developed with minimal defects occurring on the film surface during processing—negatives tend to become scratched. A slide scanner then produces a digital image. Slides were scanned at the maximum resolution. The cost of using comparable digital cameras is substantially greater.

3. Analyzing the Digital Image with the Appropriate Imaging Software. The software packages used were Adobe Photoshop to manipulate the digital images and SigmaScan Pro to derive optical density scans along selected directions. The scanned images are converted to gray scale images. This allows gray scale intensity to be measured and related to the sample concentration (see next section). A typical image contains approximately 850 × 3000 pixels. A substantial amount of noise would be present if the intensity of each pixel was measured and the computing time required would be large. Consequently, the column was divided into bands approximately 40 pixels wide. The optical density of each band is directly related to the light absorption experienced by the beam coming from the light source through the column in the direction perpendicular to the film. This is illustrated in Figure 1. The distance *OL* is twice the radial distance of the bands or 2 × 40 pixels. The optical density results

(16) Broyles, B. S.; Shalliker, R. A.; Guiochon, G. *J. Chromatogr., A.* In press.

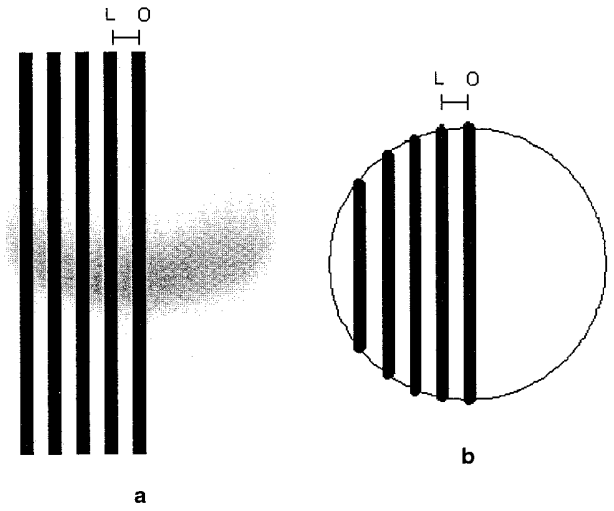

Figure 1. Schematics of the sectioning of the column. For the sake of clarity, every other section is shown on the left-hand side of the column only, beginning with the center cut. In this case, cuts made at 0.2*R*, 0.4*R*, 0.6*R*, and 0.8*R* are shown (*R* is the column radius). All cuts have the same width. A total of 19 sections were used for the complete analysis. (a) Overlay of the digital image of a zone and the vertical cuts of the five odd-ranked sections on the LHS of the column. (b) Cross section of the column with the optical axis of the system and the horizontal cuts of the five odd-ranked sections.

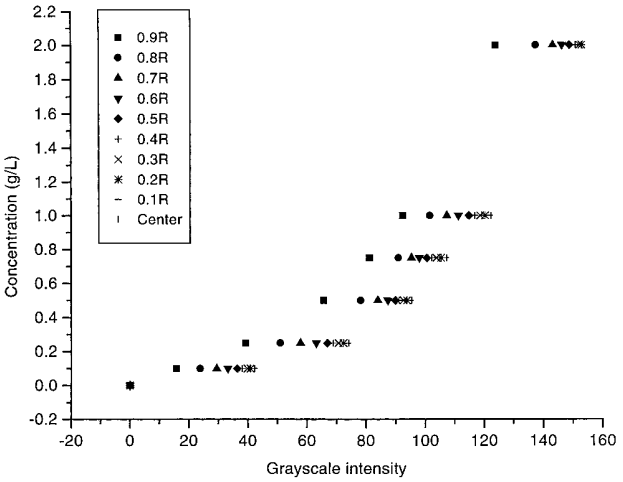

Figure 2. Calibration curves in a packed column. Nine bands on the left-hand side of the column and its center. Concentration range, 0.10−2.0 g/L.

from the absorption of the incoming light by the analyte over the entire length of the trajectory inside the packing material; i.e., it is a function of the integral of the concentration distribution along the optical path length. Conversely, from the calibration, it is possible to derive the average concentration of the analyte solution along the optical path length. This does not give, however, any information regarding any possible variation of the concentration along the optical path.

4. Determining the Detector Characteristics. These are (a) the linear dynamic range, (b) the maximum sample concentration compatible with a linear response, (c) a calibration curve derived from standards of known concentration, and (d) corrections needed to account for the variable path length of a circular chromatography column.

The column essentially behaves as an absorption cell in photometry. It is cylindrical. Consequently, the path length decreases continually from the column center to the column wall. In the column center, it is 17 mm; at the wall it is 0 mm. Since absorption is a function of the sample concentration and the path length (Beer−Lambert law), this path length change must be taken into consideration. The simplest method of doing so was to measure the absorption (or light intensity) of standards at various transverse distances.

The procedure adopted for calibration involved percolating solutions with known concentrations of iodine through the column until elution of the breakthrough curve. The column was then photographed, and the gray scale intensity along slices parallel to the central axis were measured. Plots of concentration versus gray scale intensity were then derived. A total of 19 such curves were produced, that is, a curve representing the central region of the column and a further nine curves each side of the column center at increments of 0.1 relative column radius (r/R). These calibration curves are shown in Figure 2. Unfortunately, the relationship between sample concentration and light intensity was not linear. The best-fit equation is

$$C = e^{a+b\sqrt{I}} \quad (1)$$

where C represents the concentration of the iodine (in g/L), I is the gray scale intensity, and a and b are numerical coefficients that depend on the radial location. Note in Figure 2 that the curves within the region $\pm 0.4R$ are almost coincident. The deviation increases near the wall region. The r^2 values for these correlations were all larger than 0.995.

The amount of sample injected must be small enough that the local concentration never produces a gray scale intensity higher than that recorded on the calibration plots. The chromatographic process is usually accompanied by a serious dilution of the sample. It was found that a 12 g/L solution of iodine in carbon tetrachloride always yielded a gray scale intensity well within the limitations of the calibration curve.

Figure 3 illustrates a digital image (before background subtraction; see ref 12) of a 20 μL sample of a 12 g/L iodine solution migrating along a chromatography column. The photograph was recorded 2.5 min after injection. The gray scale intensity was measured along the column length at radial increments of 0.1*R* from the column center to the column wall. These intensities were placed in a spreadsheet, which enabled the application of eq 1. As an example of the results, Figure 4 illustrates a height normalized plot of gray scale intensity (curve a) versus the migration distance along the center band of the column, while a height-normalized plot of the concentration profile versus migration distance following application of eq 1 is shown in curve b. The difference between the two curves originates from the nonlinear behavior of the calibration curve (Figure 2). The contrast illustrates the absolute need of the calibration to derive any quantitative information from the photographs of bands.

5. Evaluate the Refraction of Light. A possible source of error resulting from this experimental design is in determining the exact radial location of the band. Even very small differences in the refractive indexes of the glass column ($n = 1.473$), the

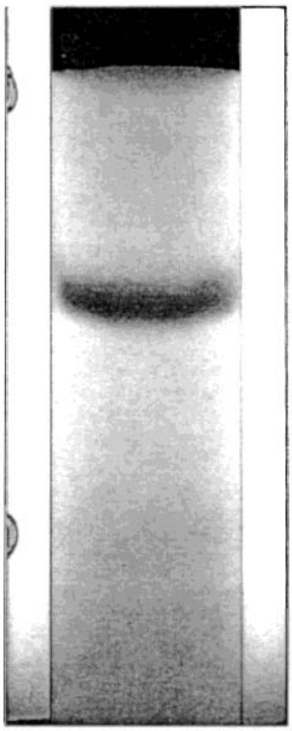

Figure 3. Photograph of an iodine zone 2.5 min after injection. Injection volume, 20 μL of a 12 g/L iodine solution in carbon tetrachloride. Flow rate, 1.5 mL/min. Shutter speed, 1/60th s, aperture *f* /16. Column fitted with a 10 μm frit.

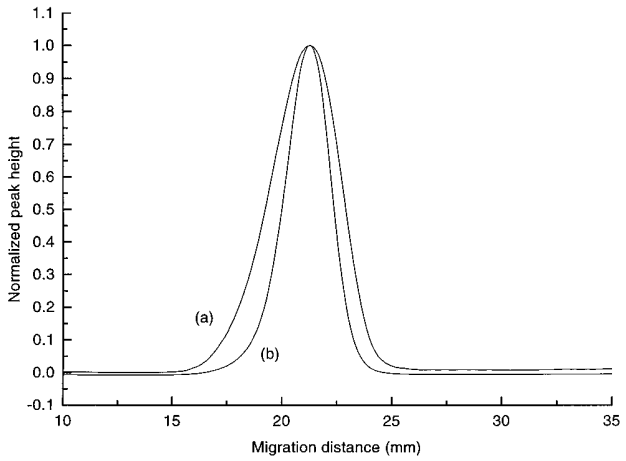

Figure 4. Height-normalized gray scale intensity profile (curve a) obtained from scanning the gray scale density of the photograph in Figure 3. Height-normalized concentration profile (curve b) derived from curve a, following standardization of the intensity profile against the calibration curves, defined by eq 1.

stationary-phase/carbon tetrachloride ($n = 1.460$) content of the column, and the solvent (dichloromethane, $n = 1.424$) in the viewing cell result in a refraction of the light and a slight shift from its incident path. A detailed analysis of the refraction of light[17] showed that this shift causes an error of less than a few percent on the radial position in the center region of the column ($\pm 0.70R$) and around 5−8% for the region between $0.70R$ and $0.95R$ (Figure 5).

(17) Broyles, B. S.; Shalliker, R. A.; Guiochon, G. *J. Chromatogr.* In press.

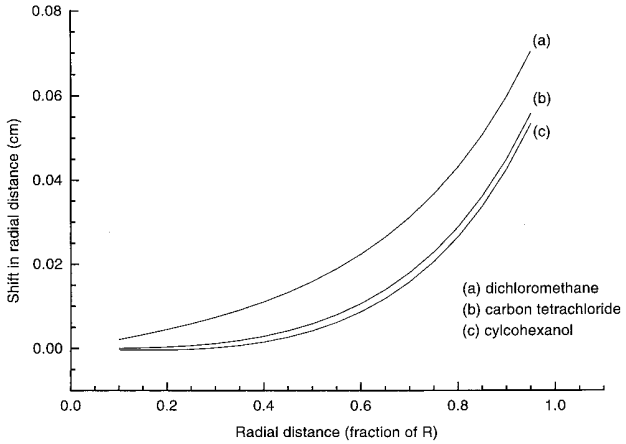

Figure 5. Influence of the refraction of light on the apparent width of the column. indexes of the fluid in the viewing cell, curve a, $n_R = 1.424$; curve b, $n_R = 1.466$; curve c, $n_R = 1.464$.

6. Normalization of the Local Amount of Sample Measured to the Amount of Stationary Phase Available in Any Region of the Column. Normalization is required when the concentration distribution of the sample across the chromatographic zone is sought. This step involves calculating the area of the column along each and any vertical column slice. The concentration distribution of the sample zone is then integrated between $l = 0$ and $l = L$, where L is the column length. The subsequent area under the curve is divided by the corresponding column section area.

CONCENTRATION DISTRIBUTIONS

In section 4 above, we compared the height-normalized zone profiles of a gray scale intensity profile to that of a concentration profile in order to illustrate the importance of accounting for a nonlinear response of the detector (see Figure 4). Using a response factor for each radial location is equivalent to normalizing the concentration profiles to the corresponding volume of the column bed examined. Once the response is integrated over each band of pixels of the digital image, the corresponding average concentration (averaged over the length of the optical path) is calculated. As long as the entire zone remains inside the column, the total area of the whole concentration distribution of the sample band is constant and proportional to the sample size. Concentration distributions in different regions indicate the distribution of the sample across the column.

As an illustration, Figure 6 shows plots of the local concentration in the sample band shown in Figure 3, along the axial direction of the column. Figure 6a shows the concentration along the 10 column bands (see Figure 1a) on the left-hand side (LHS) of the photograph (including the center slice); Figure 6b shows the same data along the 10 bands on the right-hand side (RHS) of the photograph. These concentration profiles were derived from the calibration curves shown in Figure 2. They suggest that the column is not symmetrical around the vertical plane through its axis. Important radial differences in the mobile phase velocity and the bed efficiency are visible.

From the profiles shown in Figure 6, the area under each curve can be determined to yield plots of the fractional peak area versus the radial location, shown in Figure 7. The distribution of the

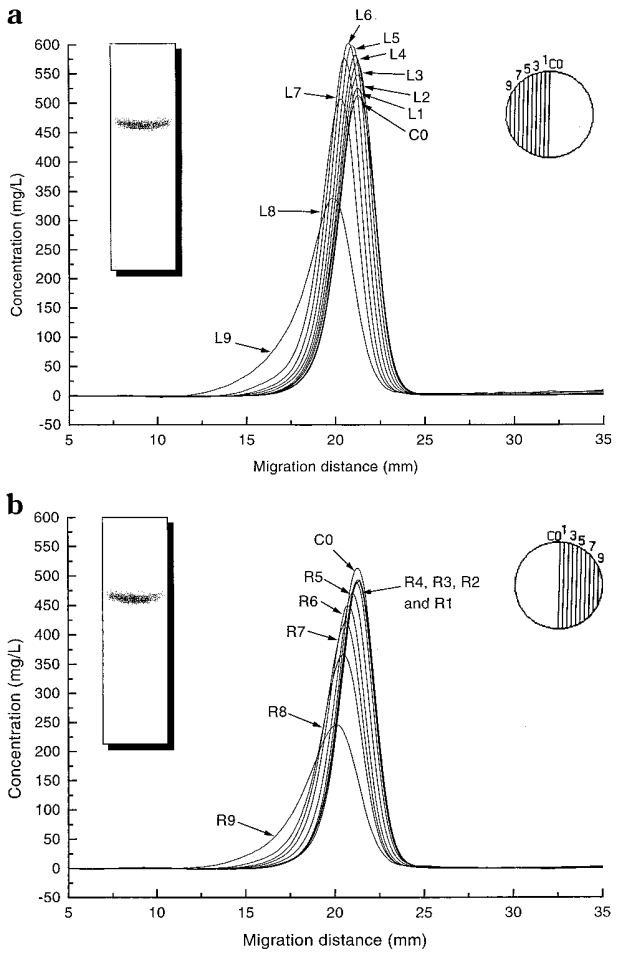

Figure 6. Comparison between the axial concentration profiles along the different vertical bands derived from the photograph shown in Figure 3. (a) Profiles from the nine column sections on the LHS and the center section. (b) Profiles from the nine column sections on the RHS and the center section.

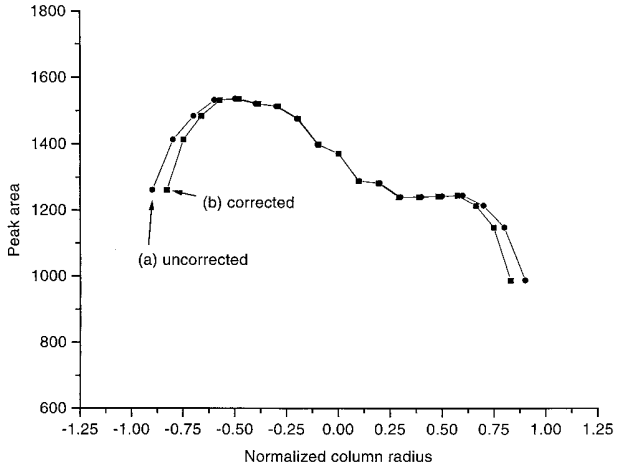

Figure 7. Peak area versus radial location. Plot derived from the concentration profiles in Figure 6. Curve a: area measured from the uncorrected zone profiles. Curve b: area measured from the refractive index-corrected zone profiles.

sample in this instance was predominately favorable to the left-hand side of the column, an effect that can also be observed in Figure 6. Also, the concentration decreases rapidly on both sides of the column in the proximity of its wall. The origin of this form of radial heterogeneity of the band is the subject of independent studies.[16,17] The importance of the correction for the refraction of light (as discussed in section 5 above) is also illustrated in Figure 7. It is insignificant, except in the immediate proximity of the column wall where it can reach 5% at radial distances in excess of 0.7*R*.

During the process of zone analysis, the profile is sectioned into transverse slices in the depth direction (i.e., parallel to the camera axis), as shown in Figure 1. In general, there are 19 slices at intervals of 0.1*R*. Each slice was between 41 and 43 pixels wide. The sectioning operation is time-consuming and tedious, particularly if high precision is required. To determine the possible influence of this error, the column sectioning was deliberately offset by 10 pixels to the right-hand side, an error far in excess of the one made under normal conditions (1−3 pixels). This offset causes an error of less than 7% in the peak area at 0.8*R*. In the central region of the column, the error made is totally insignificant.

REPEATABILITY AND REPRODUCIBILITY OF THE RESULTS

An important aspect of the application of this method of quantitative investigation of column performance through band visualization is the degree of reproducibility of the data obtained. In studying the reproducibility, several aspects must be considered: namely (1) the reproducibility of the quantitative data obtained with the slide scanner—both from slide to slide and from day to day; (2) the reproducibility of these data from slide to slide within one roll of film; and (3) their reproducibility between different rolls of film.

1. Scanner Reproducibility. One slide was scanned a total of 12 times, 3 times successively, at intervals corresponding to 3, 30, 90, and 240 min after the scanner was initialized. The process was repeated on a second day. The 12 digital images derived from the same photograph were analyzed according to the results of the previous discussion. The relative standard deviation of the peak area was 4.4% for the entire 2-day period. This study of the slide-scanning process takes into account the process of background subtraction.

2. Slide-to-Slide Reproducibility. The reproducibility of the photographic image was evaluated with respect to the peak area, the migration distance, and the column efficiency. The reproducibility of the distribution of the peak areas as a function of the radial location (e.g., data in Figure 7) was high. In the worst case, for scans made close to the column wall, the range of triplicate measurements was 9%. The retention times for each sample overlaid almost perfectly, as would be expected because small changes in color intensity would be proportional across the entire slide, hence having little influence on the location of a maximum. Deviations in the retention time are more likely to be related to small fluctuations in the solvent flow rate. Good agreement was also observed for replication of the reduced plate heights. The reproducibility was better for the half-height method than for the variance method, but even then the range of the results of triplicate measurements was less than 20% in the worst case, when the second moment was used.

3. Film-to-Film Variations. Their influence was tested by analyzing photographs of triplicate injections of the same iodine sample as above, but using a new roll of film. The results showed

some minor differences between the two photographs taken 3 days apart. Namely, with respect to the peak areas, a 24% difference was observed for regions near the wall and a 16% difference was recorded in the central region. For much of the column, efficiencies remained similar, although some notable differences were recorded on the left-hand side of the column, where the efficiency improved. We believe that most of these differences arose from the bed consolidating in the period between the two photographs were taken. The details of this study and the justification of this statement are reported elsewhere.[17] To eliminate the influence of variations from one roll of film to another, the photographs of all the experiments of each series of results reported here were made on the same roll of film.

AN APPLICATION OF ON-COLUMN VISUALIZATION

Being able to see inside a chromatography column during the experiment offers the chromatographer an opportunity to examine aspects that would otherwise be difficult to evaluate. For instance, on-column visualization lets us examine the effect of peripheral fittings on the sample distribution. Local column efficiencies can be evaluated—providing details on bed homogeneity.[12,16,17] The wall effect can be examined as can the infinite-diameter column effect.[12,18] The process of bed consolidation can be studied[19] and behavior such as viscous fingering can be observed.[13,14] In the current paper, we wish to illustrate the significance of on-column visualization by evaluating sample introduction through a column header.

Precolumn dispersion during sample introduction onto the column can have adverse effects on the chromatographic performance due to initial band broadening as the sample passes through the inlet frit and onto the packed bed and the band formed is not radially homogeneous. Typically, precolumn, on-column, and postcolumn effects are tallied together and observed in the detector response to the injection of the sample. Conventional chromatographic methods allow the estimation of the global effect of extracolumn sources of band broadening, e.g., by measuring the variance of the signal obtained by replacing the column with a zero-volume connector. However, it is very difficult, if not altogether impossible, to isolate the effects of peripheral fittings on band dispersion from those effects caused by other extracolumn phenomena. The details of the radial features of the band profile are lumped together in a single number, the increase in band variance. Consequently, on-column visualization of sample migration is particularly suited for studies of this nature.

The inlet and outlet fittings, including their frits, that were supplied with the glass column were not satisfactory. It was not possible to find a commercially available frit that exactly fitted the internal diameter of the column (17 mm). It was found too difficult to machine tool circular, homogeneous frits from sheets of stainless steel frit. The 2 and 10 μm pore size frits used were commercially available. However, there is a mismatch between their outer diameter (15.9 mm) and the column inner diameter. So, the frit had to be inserted into a head fitting made to custom.

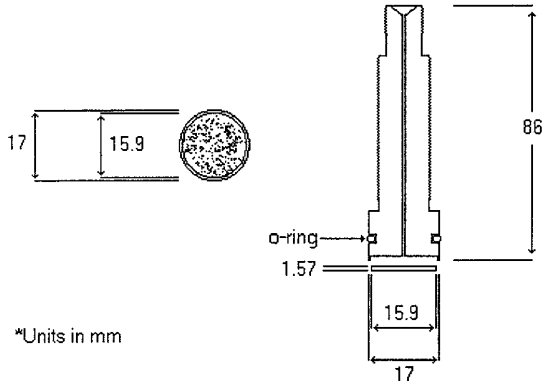

Figure 8. Diagram of the column header containing the frit.

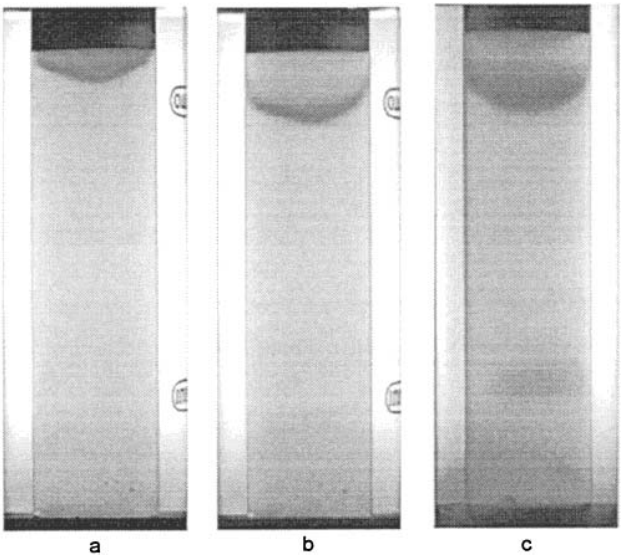

Figure 9. Photographs of the sample band eluting from the inlet of the column that contained a 2 μm frit. (a) and (b) photographed from camera 1, (c) from camera 2, at right angle to camera 1, (a) after 25 s, (b) and (c) after 60 s. Flow rate, 1.5 mL/min.

This head fitting had a recessed face machined to hold the frit firmly in place while avoiding mobile-phase leaks along the column wall, around the frit. The edge of the frit was approximately 0.5 mm from the wall of the column, with a ring of plastic from the frit holder squeezed between the frit and the column wall. This did in all likelihood influence to a small degree the "wall effect", especially in the region close to the column inlet. However, when evaluating the frit effect, the study was conducted such that measurements were made no closer than approximately 0.8R, where R is the column radius, hence, more than 1.7 mm from the column wall. The design of the head fitting is shown in Figure 8. Mobile phase and sample entered the column through a 1/16 in. hole, centered on the inlet frit. Compression of the column header against the bed ensured that the frit was tight against the header.

1. Sample Introduction through a 2 μm Frit. Two different 2 μm frits were examined. Parts a and b of Figure 9 are photographs illustrating the sample band eluting from the first of these 2 μm frits, at two different times. These results relate to

(18) Broyles, B. S.; Shalliker, R. A.; Guiochon, G. In preparation.
(19) Shalliker, R. A.; Broyles, B. S.; Guiochon, G. Visualization of Column Efficiency During Bed Consolidation in an Axial Compression Chromatography Column. Presented at the 15th Australian Symposium on Analytical Chemistry and Chromatography 99, Melbourne, July 4−9, 1999.
(20) Bird, R. B.; Stewart, W. E.; Lightfoot, E. N. *Transport Phenomena*; Wiley: New York, 1960.

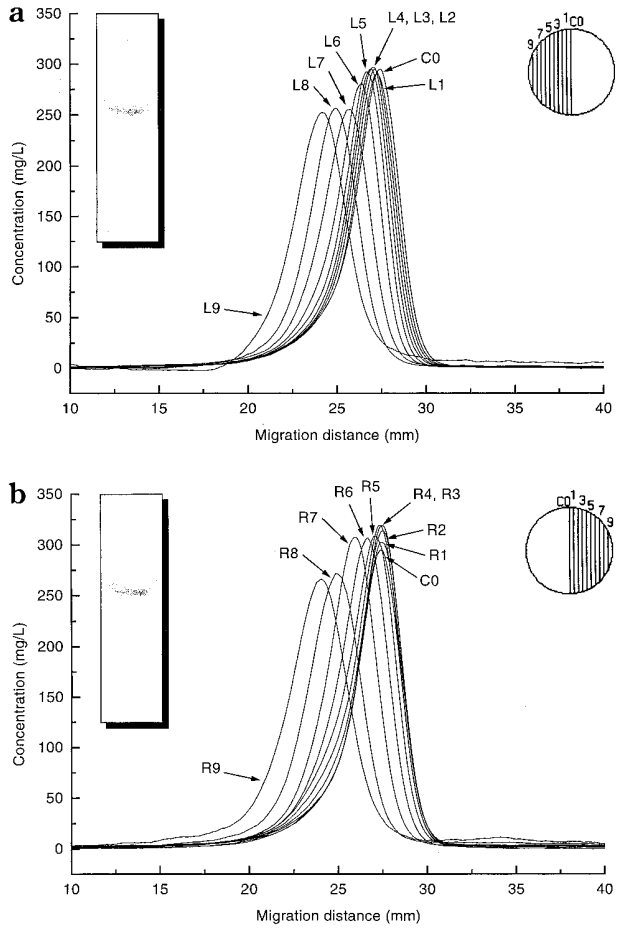

Figure 10. Migration band profiles obtained from the gray scale intensity profiles measured over the sample band illustrated in Figure 9, camera 1. (a) represents the left-hand side, and (b) represents the right-hand side. Each band (right inset) has a width of 0.81 mm (approximately 40 particle diameters). The image was divided into 19 sections radially across the column.

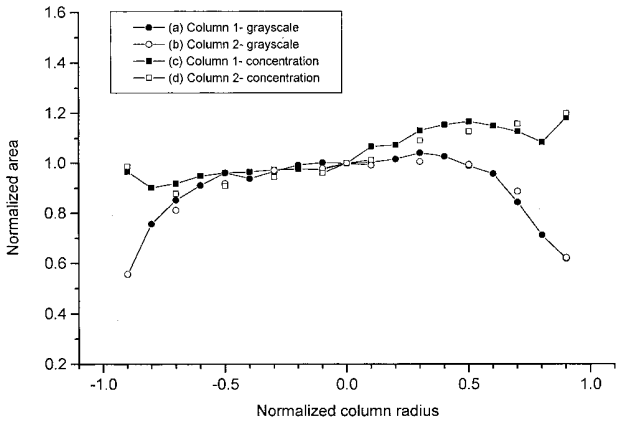

Figure 11. Area under each migration band profile normalized to the area of the central band profile, as a function of the column radius. (a) Column 1, head fitting containing a 2 μm frit, values of the gray scale intensity. (b) Column 2 same head fitting as in column 1, but on a new column, gray scale intensities. (c) Same as (a) but concentration instead of gray scale intensity. (d) Same as (b) but concentration instead of gray scale intensity.

the column designated as column 1. The symmetry of the band is verified by the photograph in Figure 9c, recorded simultaneously to the one in Figure 9b but at a right angle. The sample entered the column in the central region prior to the wall region, resulting in a curved profile. Thus, the migration distance of the profile depends on the radial position, as shown by the overlay of the migration profiles shown in Figure 10a (LHS) and b (RHS).

Clearly the central region of the sample band migrated fastest. This could have been a result of either the lack of a distributor or a heterogeneously packed bed. This was not so, as demonstrated by results shown later and obtained using the exact same frit fitted to a column of poorer efficiency, but yielding an almost exact migration profile. Also, studies with 10 μm frits add support to the effect being irrespective of the column. *We attribute this effect to a radial heterogeneity of the inlet frit itself*, probably as a consequence of its manufacturing process. Since the inlet and outlet pressures are the same over the entire respective cross sections of the column, radial differences of the local velocities can be explained only by a radial distribution of the local permeability. The permeability is lower in the peripheral region, and consequently, the sample arrives later along the wall than in the central region, as can be seen in Figure 10. Figure 11 shows the plots of normalized area of the gray scale intensity (circles) and the concentration (squares) versus the normalized column radius. In this figure, the area of the concentration profile of each radial section was normalized to the area of the concentration profile for the central section of the column. These plots therefore reflect the distribution relative to the column axis. The radial distribution of the gray scale intensity suggests an uneven radial distribution with a concentration lower in the wall than in the central region (lower curve). This conclusion would be incorrect. It is a consequence of the strongly nonlinear calibration curve (Figure 2). As the upper curve in Figure 11 shows clearly, the sample distribution was slightly heterogeneous across the column, with a bias toward the right region on the figure. This result demonstrates the absolute need of calibration and the inability of the eye to make quantitative judgments. It also illustrates the good reproducibility of our procedure for column packing. Finally, it shows the rather serious lack of homogeneity of the frits used in chromatography.

The migration profiles obtained with our procedure allow the determination of local axial dispersion coefficient and the evaluation of the column efficiency along each stream path, averaged over the migration distance considered. Using the number of theoretical plates derived from the peak width at half-height of the axial concentration profiles, a plot of h versus the normalized column radius (Figure 12, curve a) can be derived. This plot shows that the column is reasonably homogeneous and, with $h = 2$, quite efficient in the central region. However, the efficiency decreases markedly toward the wall. Coincidentally, perhaps, the region of low efficiency on the RHS of the column ® > 0.5 R) correlated to the region of higher sample concentration observed in Figure 11. The mean local value of h was 2.7, which verifies that well-packed columns are obtained, despite the low packing pressures that had to be employed in this study, using glass columns. Because of the parabolic profile of the concentration distribution at the inlet fitting (Figure 9), the overall "on-column" sample band profile obtained by summing the contributions from the individual sections yielded a reduced plate height of 5.2 (from peak width at half-height). Further results (not discussed here) falsified our

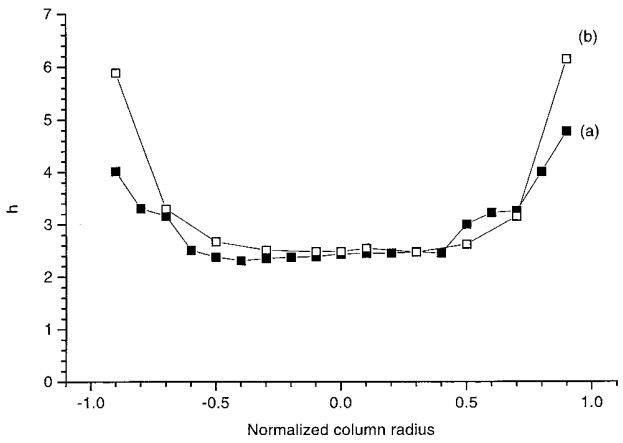

Figure 12. Reduced plate height versus the radial location. (a) For column containing the 2 μm frit from which the photographs in Figure 10 were obtained, column 1. (b) Reproducibility of the 2 μm frit; the reduced plate heights were obtained from a second column containing the same frit, column 2.

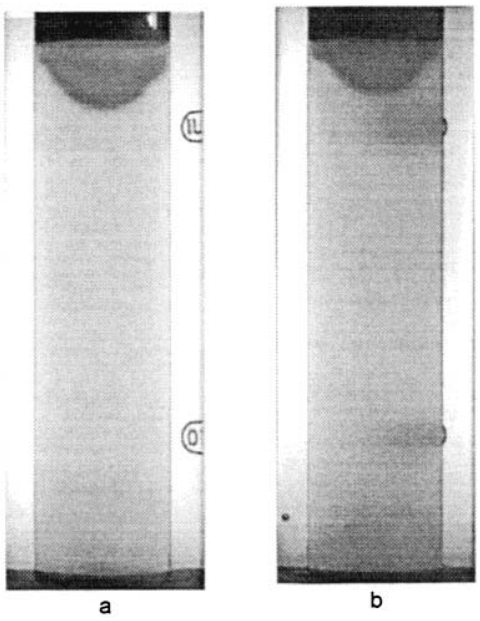

Figure 13. Photographs of the sample band eluting from the inlet of the column that contained a second 2 μm frit. (a) camera 1 and (b) camera 2, both after 42 s; the cameras were mounted at right angles to each other. Flow rate, 1.5 mL/min.

own initial assumption that the design of the outlet fitting was unimportant. On the contrary, the outlet fitting also influences the peak shape to a large degree.

Consequently, regular detector responses do not reflect correctly the true band profile and compared poorly to the elution signals obtained by proper integration of the "on-column" band profiles. In a subsequent study,[17] we compared the elution profile obtained by integration of the on-column migration profiles to that recorded from a regular on-line detector analyzing the bulk eluent at the column exit. The agreement was reasonable, but differences did exist that are due in most part to the influence of the outlet fitting. This is why we did not show conventional detector-generated responses in this study. In a future communication, we will address this problem in more detail.

A second column (labeled column 2) was prepared using the same frit from which the images shown in Figure 9 were recorded. The results were similar to those just described for column 1 for the sample gray scale intensity concentration distributions (Figure 11) but not for the column efficiency (Figure 12, curve b). However, these differences relate to the column performance, not those of the inlet frit. For instance, the plot of h versus the normalized column radius is higher for column 2 than for column 1 in the region close to the wall (Figure 12, curves b and a, respectively). From this plot some doubt could remain regarding whether the column was the cause of the poor performance or whether it was the frit itself. However, examination of Figure 11 shows that the sample distributions on both columns were in excellent agreement. Furthermore, both columns exhibited almost exactly the same normalized migration rates (results not shown). In addition, if the reduced plate height of each column was normalized and plotted as a function of the column radius, we see that the sample introduced into the second—more poorly performed—column migrated with a more uniform efficiency than that in the first column (results not shown). These results confirm that the frit delivered sample in a reasonably reproducible manner from one column to another, with minor differences due to the asymmetry of the frit and the fact that the second set of results were analyzed from only one of the camera angles.

The behavior of a second 2 μm frit was evaluated on a third column. The photographs in Figure 13 show the profile of the sample distribution at the column inlet. This profile was more strongly curved than the previous ones. More importantly, however, visualization from two orthogonal angles (parts a and b of Figure 13 represent photographs taken simultaneously) verified that the sample band entered the column slightly off center, illustrating the heterogeneous nature of the frit. Again, these images show the importance of a multiaspect visualization technique (although the observer can turn around the column, it is difficult to see two images at once). As a consequence of the off-centerness of the injection, the column efficiency was found to be poor, with some peak splitting being observed when the concentration profiles were measured along the different parallel flow streams (not shown). This prevented the acquisition of any meaningful information regarding the column efficiency.

2. Sample Introduction through 10 μm Frits. Parts a and b of Figure 14 are photographs illustrating the introduction of an iodine sample entering into the column through a 10 μm frit. The photographs in parts c and d of Figure 14 were recorded at exactly the same time as those in parts a and b, respectively, but at right angles. Their comparison verifies the symmetry of the injection plug. In this instance, the sample band was nearly flat and pluglike. The sample concentration appeared to be uniformly distributed across the column. The migration profiles shown in Figure 15a (LHS) and b (RHS) illustrate that the sample band moved through the frit and the head of the column at a constant velocity. Note that the hump on the baseline, in the rear of the profile, is a result of a discoloration of the column background, an artifact of the photographic process, and it does not migrate during the course of the experiments. Note also that the radial concentration distribution is the reverse of that observed with the 2 μm frits. The area of the migration profiles in Figure 15 increases with increasing radial distance, by contrast with what is seen in Figure

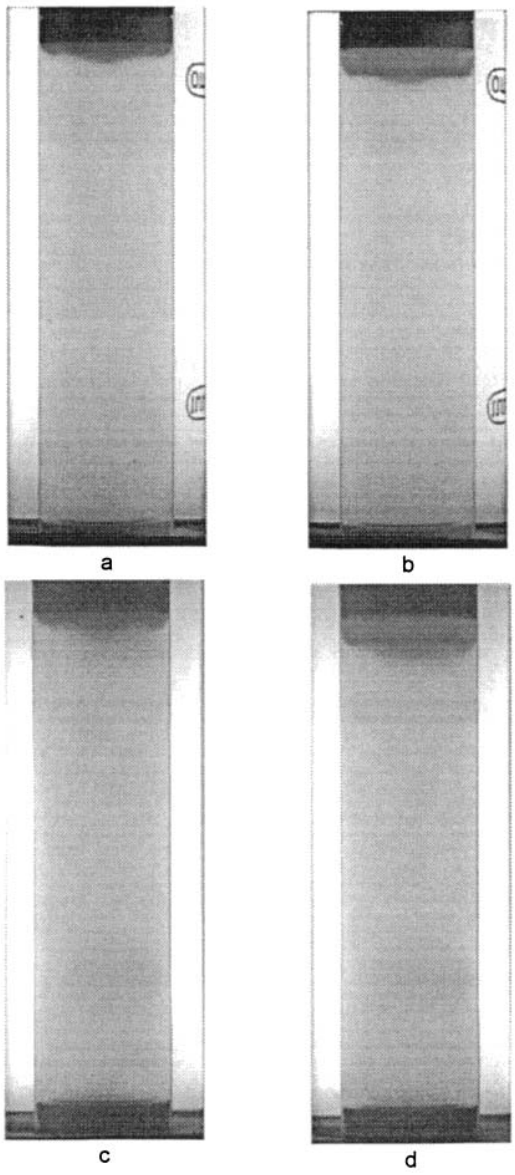

Figure 14. Photographs of the sample band eluting from the inlet of the column that contained a 10 μm frit. (a) and (b) photographed from camera 1 after 18 and 30 s, respectively, (c) and (d) from camera 2, at right angle to camera 1, in the same time as (a) and (b), respectively. Flow rate, 1.5 mL/min

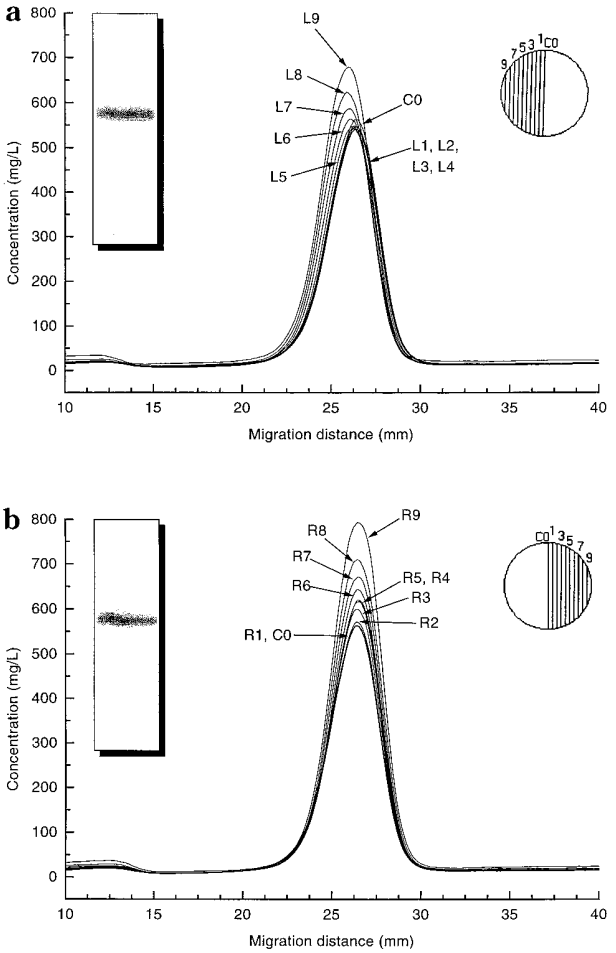

Figure 15. Migration band profiles obtained from the gray scale intensity profiles measured over the sample band illustrated in Figure 14, camera 1. (a) represents the left-hand side and (b) represents the right-hand side. Each band has a width of 0.81 mm (approximately 40 particle diameters).

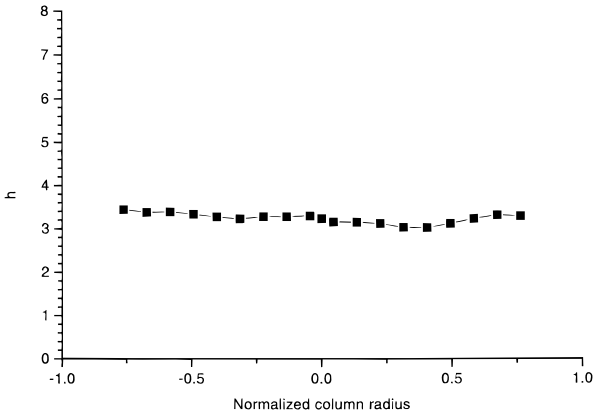

Figure 16. Reduced plate height versus the radial location for the column containing a 10 μm frit from which the photographs in Figure 14 were obtained.

10. The average sample concentration is highest in the area nearest the column wall and lowest in the central region.

The efficiency measurements (Figure 16) derived from the concentration profiles in Figure 15 show that the column bed was essentially homogeneous radially. The mean value of h derived from the width of the peaks at half-height was 3.2, somewhat higher than in previous cases. The inlet fitting did not initiate a heterogeneous distribution of the radial migration velocity of the solute, despite the nonuniform concentration distribution. The overall migration profile obtained by summing the 19 individual profiles is uniform and nearly symmetrical, as would be expected given the overlaid profiles shown in Figure 15. The efficiency measured from this profile was $h = 3.3$ with the half-height method, practically equal to the mean value of the individual sections. This value of the overall column efficiency is higher than those obtained for the 2 μm frit.

Several other 10 μm frits were tested to determine the degree of repeatability of the frit performance. None gave better overall performance than the one described above (Figures 14−16). In

general, the other 10 μm frits produced a variety of weakly curved elution profiles. Only in one instance, however, did we observe sample introduction through a 10 μm frit that was poorer than through the best 2 μm frit. A comparison between the performance obtained with different frits relies on the assumption that the other factors influencing the terms of comparison remain constant. A new column had to be made each time the frit was changed. It must be assumed that the performances of all these columns were nearly the same and that small variations did not effect the sample introduction. The results of several experiments make us confident that such variations did not influence the results.

For example, in a series of experiments carried out to examine this effect, we were able to test one frit, remove the head fitting, test a second, poorly behaved frit, then remove the head fitting once again, and retest the original frit. We found that the first frit gave similar band profiles during the first and third tests, profiles which were significantly different from that of the second frit in the second test. This procedure could not be used routinely, however, as the success rate of removing the column header without destroying the bed was low. Overall, the 10 μm frits proved to lead to markedly higher efficiency peaks through less intense extracolumn band broadening and less tailing of the elution band. Since the radial distribution of the local efficiency across the column remained constant from column to column, the significant differences observed between the results obtained with the different frits must originate from the frit permeability, which controls the radial distribution of the flow velocity of mobile phase into the column. If the frit permeability is low, there is a serious risk of leaks bypassing the frit entirely and leading to an heterogeneous sample distribution affecting negatively column performance.[17] If the frit permeability is closer to that of the bed, the effect is less dramatic. Still, the homogeneity of the frit is of great importance. To this end, the 10 μm frits tended to behave much better, but even so, variations from frit to frit were significant.

CONCLUSION

Multiaspect visualization is a valuable technique for studying sample distribution throughout the column. Considering only a single aspect of the concentration distribution in the column may cause decisions based on misleading information regarding the flow profile of the sample band. For example, a sample that appeared to enter the column centrally from one aspect was in fact entering off-center when viewed from the perpendicular direction. Profiles that appear flat, but disperse, can in fact be shown to be entering the column heterogeneously. Hence, this visualization technique provides the chromatographer with a valuable means of evaluating, among other things, the performance of head fittings.

The 10 μm frits produced better band profiles than the 2 μm frits. This result is in a large part a consequence of the choice of a material with 21 μm average particle size to pack the columns. Larger particle beds require coarser frits, smaller particles, finer ones. The selection of the frit size cannot be made entirely independently from the selection of the distributor.[16] In all this work, no distributors were used. It is thus remarkable that entrance profiles as flat as those illustrated in Figure 14 could be obtained. This illustrates the important role that a frit appropriately chosen may have on the homogenization of the distribution of the sample concentration at the column inlet.

Finally, most of us purchase our frits and fittings from a supplier, who we believe in good faith offers a product of unquestionable reliance. For the most part, this is true. But, even unbeknownst to themselves, manufacturers may deliver products that do not attain the level of performance that is expected. Putting the product to the test using a technique such as the one described here illustrates how important it is to evaluate even the given. Frits are the product of an industry more oriented toward the manufacturing of filters than that of distributors for the inlet of chromatographic columns. The only test made on frits aims at measuring the size of the largest hole, not their homogeneity. How many *f* chromatographers have made poor columns in their own laboratory because of a wanting frit?

ACKNOWLEDGMENT

This work was supported in part by Grant DE-FG05-88ER13859 of the U.S. Department of Energy and by the cooperative agreement between the University of Tennessee and the Oak Ridge National Laboratory.

Received for review April 13, 1999. Accepted September 2, 1999.

AC990370+